Available online at www.sciencedirect.com
SCIENCE DIRECT®
Journal of Nuclear Materials 342 (2005) 179–187
journal of nuclear materials
www.elsevier.com/locate/jnucmat

The reaction of water on polycrystalline UO_2: Pathways to surface and bulk oxidation

S.D. Senanayake [a], R. Rousseau [b], D. Colegrave [b], H. Idriss [a,*]

[a] *Materials Chemistry, Department of Chemistry, University of Auckland, Rm.527A, Private Bag 92019, Auckland, New Zealand*
[b] *Present address: Institut des Sciences de l'Ingénieur de Toulon et du Var, BP56, 83162 La Valette du Var cedex, France*

Received 8 February 2005; accepted 14 April 2005

Abstract

The reaction of polycrystalline uranium dioxide with H_2O is studied by in situ Raman spectroscopy, temperature programmed desorption (TPD) and X-ray photoelectron spectroscopy (XPS). The difference between UO_2 and U_3O_8 can be seen in the bulk by XRD and Raman and on the surface by both the core level and valence band regions. In the valence band region the U 5f line was far more pronounced for UO_2 than for U_3O_8. It was possible to monitor the near surface oxidation of UO_2 to U_3O_8 by H_2O at 300 K using Raman spectroscopy while oxygen deposition was quantified using XPS. TPD of D_2O on H_2-reduced U_3O_8 ($\approx UO_2$) showed desorption of D_2. D_2 desorption occurred in two temperature domains (at ≈410 K and ≈570 K). Increasing the surface exposure to D_2O affected the distribution of both D_2 peaks. The first desorption-peak populated first while at relatively higher D_2O exposure the second desorption peak increased considerably in intensity. The second desorption of D_2 during D_2O-TPD can be tracked down to oxidation of deeper layers.

1. Introduction

The surface chemistry of uranium oxides has been the focus of several studies in the last few years [1–15]. The rich chemistry associated with the uranium oxides stems from their numerous complex phases, with the most thermodynamically stable phases being UO_2, U_3O_8 and UO_3. Uranium dioxide as a major component of nuclear fuel has been under close chemical scrutiny; in particular with relation to aspects of the storage of spent and excess nuclear materials over long periods of time for safe radioactive decontamination. The oxidation of UO_2 surface is known to result in a bulk transformation first to U_3O_7 then to U_3O_8 and this process is associated with a volume expansion of 35% [16,17]. This requires careful design and engineering for permanent fuel storage to avoid further complications that may arise over long periods of time. The abundance of water in nature and its influence on all aspects of chemistry is clear and promotes great interest with relation to its chemical interactions with solid surfaces [18]. The reactions of water on uranium oxides have been undertaken in several works over single crystal [3,11,12], thin film [19], and polycrystalline surfaces [13–15] with observation of thermally activated evolution of hydrogen over

* Corresponding author. Tel.: +64 9 373 7599; fax: +64 9 373 7422.
E-mail address: h.idriss@auckland.ac.nz (H. Idriss).

0022-3115/$ - see front matter © 2005 Elsevier B.V. All rights reserved.
doi:10.1016/j.jnucmat.2005.04.060

oxygen defected/reduced UO_2 surfaces. Results have shown that the reduced UO_2 surface is oxidized upon reaction with water as has been observed on oxygen defected $UO_2(111)$ [3] and on $UO_2(100)$ [11,12] single crystals.

Raman spectroscopy is commonly used as a bulk characterization technique to identify solid materials. Several studies have been previously undertaken using the Raman microscopy technique for the characterization of the U–O system [20–28] but few have focused attention to the oxidation and reduction mechanisms associated with these materials [28]. UO_2 has a fluorite structure with a space group of O_h (Fm3m) and group theory predicts [29] two vibrational modes of $T_{2g} + T_{1u}$. The T_{2g} (triply degenerate) mode is Raman active while T_{1u} is Infrared active [22]. Tri-uranium octaoxide (U_3O_8) is intermediate in oxidation between UO_2 and UO_3. It has many known crystalline forms α-U_3O_8, α'-U_3O_8, β-U_3O_8, and γ-U_3O_8 of which α-U_3O_8 is the most stable. Its complex structure has been previously studied by several models including those of Loopstra (using neutron diffraction [30]) and Ohwada and Soga with approximate coordination analysis [31] to an ever-complicated array of vibrational assignments that is as yet not complete. Butler et al. have endeavored to complement theoretical calculations using the models of Loopstra and Ohwada with experimental Raman spectra [20]. In this work we have studied the reaction of H_2O-vapor over the surface of polycrystalline UO_2 using X-ray photoelectron spectroscopy, temperature programmed desorption and micro Raman spectroscopy techniques in an effort to understand the dynamic of surface mediated oxidation of UO_2 to U_3O_8 upon contact with H_2O vapor.

2. Experimental

The Raman spectroscopy was carried out using a Renishaw 1000 Raman Microscope. A blue laser was used at 488 nm as the excitation source with an operation power of 20 mW, and a red laser was also used where specified for single crystal samples at 786 nm with an operation power of 26 mW. The spectra were obtained at an exposure of 20 s on an extended shift of 100–4000 cm^{-1}, with multiple scans co-added to ensure maximum sensitivity. The laser was focused onto the sample using 50× and 20× uncoated-objective lenses, at a sample spot size of ≈1 μm. Primarily the Raman laser was calibrated using a calcite crystal (1086 cm^{-1}), and the correct shift is maintained for all the oxide samples. During the start of all Raman scans a cosmic ray subtraction is automatically carried out to account for any radioactive interference from the immediate atmosphere. A Linkam THMS 600 hot/cold stage was used to maintain the uranium oxide samples in situ, while being heated under H_2/O_2 environments, at 1 atmosphere. The stage is water-cooled and temperature controlled using an interfaced programmer. Small glass windows were used for the reflectance of the laser beam. The samples for this experiment were made by primarily pressing technical grade α-U_3O_8 into discs of ∼1 mm thickness. Thus once inserted into the stage, introduction of degassed H_2O vapor was performed by way of injections of 1 ml from a degassed (oxygen-free) H_2O vial through a septum attached on to the stage.

Hydrogen-reduced and oxygen annealed U_3O_8 samples were also characterized using X-ray diffraction (XRD) prior to experimentation to confirm the total transformation to UO_2. The XRD spectra were collected using a Phillips 1130 generator and a Philips 1050 goniometer (X-ray source Cu tube Kα 0.1514 nm, 44 kV, 20 mA) at an operating speed of 2° $2\theta\,min^{-1}$.

X-ray photoelectron spectroscopy is undertaken in a stainless steel ultra high vacuum (UHV) chamber (1×10^{-10} Torr) Perkin–Elmer (PHI) equipped with surface analysis and sputtering equipment as described elsewhere [3]. The XPS experiments were undertaken with Al Kα radiation source (1486.6 eV ($h\nu$), 240 W, 14 kV) at room temperature with the sample at 45° from the X-ray source. The polycrystalline samples are mechanically pressed into 0.5 mm thick pellet and mounted onto stainless steel stubs and pretreated (where described) in a pre-chamber (base pressure less than 5×10^{-9} Torr) and placed onto 360° carousel/rotatable turret prior to scanning. Scans of the samples are undertaken at 25–50 eV pass energy, 350 ms per step, 0.1 eV per step, and with 15–30 co-added scans. Sample preparation involved sputtering with Ar^+ (3–5 keV, 20 mA) and annealing to high temperatures (800 K) for several hours to undergo reduction (where applicable) and clean samples from impurities. The adsorption of H_2O is undertaken from a pyrex vial attached to a leak valve and a stainless steel dosing arm adjoining the UHV chamber, which is pumped to 10 mTorr with a roughing pump. Dosing of H_2O is performed at room temperature by positioning sample in front of a dosing needle.

Temperature programmed desorption (TPD) is undertaken in a smaller high vacuum chamber (1×10^{-7} Torr) equipped with a Leda–Mass quadrupole mass spectrometer and pumped with a diffusion pump. The vacuum chamber is connected through a leak valve to a glass manifold with a roughing pump. A 'U' shaped quartz reactor with specially fitted porous sinter to allow for powder sample to rest on and for gases to flow through is connected to the manifold together with a Cajon fitted septum for injections of D_2O (99.96%, obtained from Aldrich Chemical Co) with a SGE 1 μL syringe. 1 μL of D_2O contains 5.522×10^{-5} mol or 3.33×10^{19} molecules (density of D_2O = 1.44 $g\,mL^{-1}$). A Lindberg blue high temperature oven is placed around the U reactor and ramped linearly (0.25 K/s) during

TPD experiments. Preparation of powder samples was performed in the same experimental setup prior to experiments. α-U_3O_8 (BDH Chemicals Ltd.) was cleaned by annealing under O_2 to 773 K for 4 h. UO_2 was formed from α-U_3O_8, by annealing to 773 K under H_2 flow (≈20 ml/min, 1 atm) for 10 h.

In order to calculate the area of the peaks a calibration of the mass spectrometer had to be done in order to differentiate the contribution of water (H_2O) from that of DO for *m*/*z* 18. For this calibration D_2O was introduced into the mass spectrometer to see the variation of *m*/*z* 17, 18 and 20. The ratio $\frac{m/z18}{m/z17} = 3$ before the injection of D_2O gives the background contribution of water inside the high vacuum mass spectrometer chamber. The contribution of DO (from D_2O) can be calculated after subtraction of H_2O contribution based on *m*/*z* = 17. The remaining ratio could then be calculated; $\frac{D_2O}{DO} = 5$.

3. Results and discussion

The results will be presented as follows. First, the characterization of UO_2 and U_3O_8 samples by Raman followed by monitoring the effect of water on the oxidation of UO_2. Second, XPS of the core levels of UO_2 and U_3O_8 before and after H_2O exposure in order to quantify the amount of oxygen deposited and associated changes. Third, TPD of D_2O on UO_2 showing the associated D_2 evolution, due to water dissociation and oxygen deposition.

Fig. 1 details the characterized Raman spectra of polycrystalline UO_2 and α-U_3O_8 undertaken using the blue laser (488 nm). The experiments conducted on polycrystalline samples using the red laser (786 nm) yielded indistinguishable weak spectra possibly due to fluorescence of the sample.

The vibrational assignments for U_3O_8 are relatively complex. The most commonly accepted structure for α-U_3O_8 consists of a pentagonal bi-pyramidal structure [32]. The α-U_3O_8 spectrum in Fig. 1 is in good agreement with the results of Butler et al. [20] and Palacios et al. [23]. Table 1 details the vibrational assignments of 340, 405, 480 cm^{-1} peaks corresponding to A_{1g}, A_{1g} and E_g (U–O) stretching, respectively. Peaks at 640 and 795 cm^{-1} were collectively identified as overtones of the A_{1g} and E_g stretches (235, 342, 405 and 480 cm^{-1}). The peak observed at 235 cm^{-1} is left unassigned, as it does not fit this model or any of the other available models; this peak was also observed and unassigned by other workers [20,28].

The UO_2 spectrum is far simpler in nature as only a single fundamental vibrational stretch is expected of the T_{2g} U–O and is seen at 450 cm^{-1}. This peak is a triple degenerate (*T*), symmetric (g) stretching mode that arises as a result of the fluorite structure of UO_2. The surrounding eight O atoms for U gives a space grouping

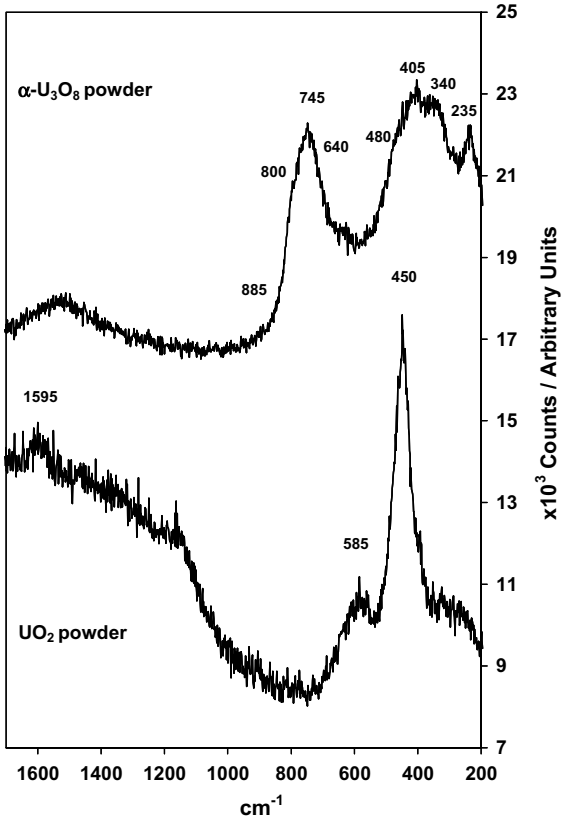

Fig. 1. Raman vibrational spectra using 488 nm blue laser of polycrystalline UO_2 and α-U_3O_8.

of O_h, that predicts two vibrational modes; the T_{2g} + T_{1u}. The peak at 585 cm^{-1} has been seen by other workers. It is not that of stoichiometric UO_2, but is a result of a damaged UO_2 matrix, and is thus a possible expression of bulk defects resulting in a breakdown of selection rules.

The UO_2 single crystal spectra using the blue laser share similar peaks of 450 and 585 cm^{-1} with that of polycrystalline UO_2 (Fig. 2). Although the 585 cm^{-1} peak appears composed of two peaks (a shoulder at the high frequency side). The main difference is however seen for the 1150 cm^{-1} peak that was not noticeable in the case of the polycrystalline oxide. This 1150 cm^{-1} stretch has been observed by Graves [22] on UO_2 single crystal, Schoenes [24] and Manara et al. [28] on polycrystalline UO_2; all using a 514 nm laser and subsequently attributed this artifact as due to electron scattering explained by a crystal field transition $\Gamma_5 \rightarrow \Gamma_3$. The 930 cm^{-1} peak cannot be assigned at present as it has not been identified on other works nor from theoretical models. Using a weaker excitation source (the 785 nm laser) resulted in similar peaks but with different relative intensities. The largest intensity is now the

Table 1
Raman spectra peak assignments of polycrystalline UO_2, U_3O_8 and UO_2(111) single crystal

Raman shift (cm^{-1})(±2)	Assignment
UO_2 polycrystalline	
450	T_{2g} U–O stretch
585	[a]
1595	1150 + 445 = 1595
Raman shift (cm^{-1})(±5)	Assignment
U_3O_8 polycrystalline	
235	?
340	A_{1g} U–O stretch
405	A_{1g} U–O stretch
480	E_g U–O stretch
640	235 + 405 = 640
745	340 + 405 = 745
800	340 + 480 = 820
885	405 + 480 = 885
Raman shift (cm^{-1})(±2)	Assignment
UO_2 (111) single crystal	
450	T_{2g} U–O stretch
585	[b]
920	450 + 450 = 920
1150	[b]

[a] Due to a damaged matrix.
[b] Electron scattering, see text for more details.

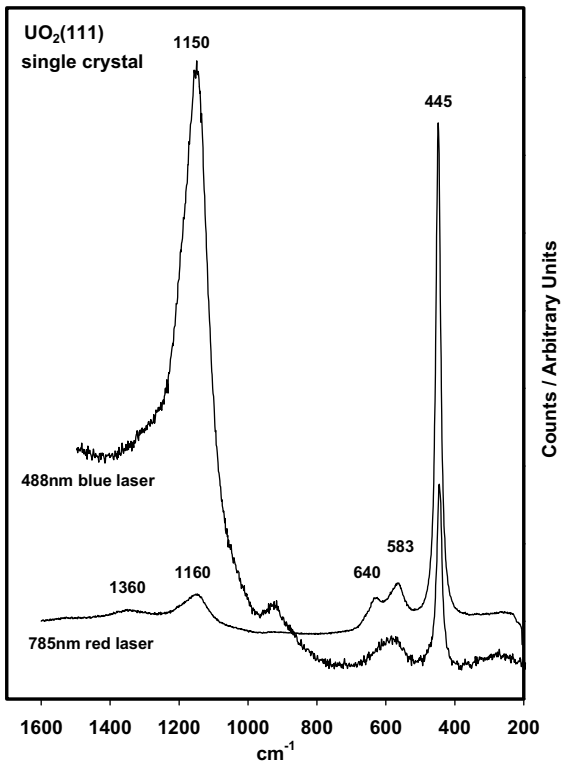

Fig. 2. UO_2 (111) single crystal Raman vibrational spectra using 488 (blue) and 756 nm (red) lasers.

fundamental 451 cm^{-1} stretch with the 1150 cm^{-1} peak much smaller in intensity. The peak at 585 cm^{-1} has de-convoluted to two peaks at 578 and 640 cm^{-1}.

Fig. 3 details the in situ micro-Raman spectra of H_2O oxidizing polycrystalline UO_2 to U_3O_8. These spectra in comparison to those in Fig. 1 exhibit a far weaker absorbance. This is due to the attenuation caused by the cell windows. The first spectra is clearly that of UO_2 (a peak at 458 cm^{-1}), upon injection of 1 mL of gas phase H_2O (1.6×10^{-6} mol) the peak at 450 cm^{-1} became broader due to the development of other peaks at the low wavenumber side. Equally important is the appearance of a peak at ~756 cm^{-1} characteristic of α-U_3O_8 (compare to Fig. 1). Doubling the amount of H_2O doubled the intensity of the 756 cm^{-1} peak (while 3 ml of H_2O also resulted in a further enhancement of the peak). This experiment confirms that at least part of the near bulk of polycrystalline UO_2 has been partially oxidized to α-U_3O_8.

Upon visual investigation of the surface using the Raman optical Microscope (Leica DMML) it is possible to distinguish the formation of several darker regions of U_3O_8 and further confirmed using Raman. These regions are not consistently formed throughout the powder surface but appear with a degree of in-homogeneity mixed with large areas of UO_2. Fig. 4 shows one representative image of these regions undertaken at 500× magnification with the lighter golden areas specifying the areas of U_3O_8 and the darker regions of UO_2. The cross hairs of the image detail the point at which the Raman spectra were extracted. It has to be noted that the color of UO_2 is normally a light brown darker than the green/grey color of U_3O_8 however under the microscope it appears as the opposite due to the illumination of the light onto these regions.

XRD did not show much change before and after H_2O adsorption, figures not shown for simplicity, they are identical to those reported for UO_2 elsewhere [4,10]. This may indicate that the main bulk of the material has not been oxidized. Another possibility is that the bulk of the oxide that has been oxidized due to the contact with water does not diffract well. The activation energy, E_d, for atomic O diffusion in UO_2 computed from [33] is equal to 177 kJ mol^{-1} while the pre-exponential term, D_0, is found equal to 3.59×10^{-3} cm^2/s. These values are taken from three measurements between 878 and 1023 K. Assuming that these are still valid at lower temperatures the diffusion coefficient, $D_{310\,K}$, was estimated and found equal to $\approx 5.2 \times 10^{-33}$ $cm^2 s^{-1}$ far smaller than XRD sensitivity.

XP spectra of Fig. 5 show the powder samples of U_3O_8 and Ar^+ sputtered U_3O_8(≈UO_2). We have previously studied the XPS core level of this system [10]. Both H_2-reduction and Ar^+-sputtering gave similar results: a

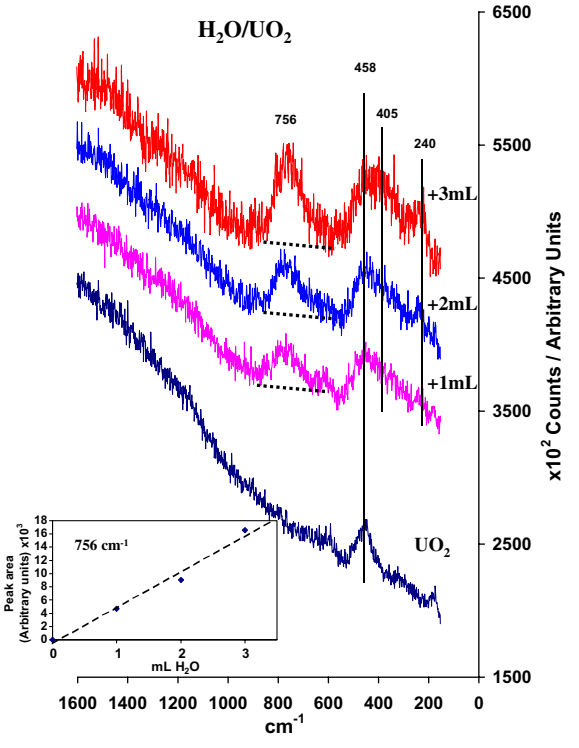

Fig. 3. In situ Raman spectroscopy experiment of H_2O vapour oxidation of UO_2 to U_3O_8. Scans performed with incremental exposure of H_2O (gas phase 1–3 ml injections). Inset shows the gradual increase of 756 cm^{-1} peak increasing with H_2O injection.

reduction of U_3O_8 to UO_2 (or very close to UO_2). The variation between the two samples is distinguishable from the difference in position of the $U4f_{7/2}$ and $U4f_{5/2}$ peaks, with the XPS $U4f_{7/2}$ and $U4f_{5/2}$ for U_3O_8 at 381.5 eV and 392.4 eV, respectively (the FWHM for the $U4f_{7/2}$ = 2.52 eV). These peaks are due to contributions from U^{4+} to U^{6+} in a 1 to 2 ratio (U_3O_8 is a mixed valent oxide). The fitting of U^{4+} and U^{6+} XPS 4f was conducted using the binding energy and FWHM from UO_2 and UO_3 (2.1 eV (10)), respectively. We have not considered the small contribution of U^{4+} satellites, though. The Ar^+ sputtered sample shows a considerable shift to a lower binding energy; the $U4f_{7/2}$ has shifted to 380.1 eV and the $U4f_{5/2}$ to 390.5 eV. The shift to lower binding energy is associated with a considerable reduction of the FWHM of the peaks (that of $U4f_{7/2}$ is = 2.2 eV). The reduction can also be followed by integrating the XPS O1s to XPS U4f (including the satellites in the case of U4f) peak areas ratios. Atomic sensitivity factors (with respect to fluorine) can be taken from Φ (XPS reference [34] for an X-ray source at 54.7° from the analyzer). It is equal to 0.7 for O and 10.3 for U (or a correction factor of 14.5). These numbers are however empirical and very sensitive to the type of analyzer and sample position. If we take the U_3O_8 that has been annealed at 773 K in high vacuum as the pure starting material the non-corrected O to U ratio is found equal to 0.165 (giving a correction factor of 16.1). On the other hand the XPS core and valence band levels of the Ar^+-sputtered U_3O_8 are very similar to those of UO_2(1 1 1) single crystal and one can also take the O

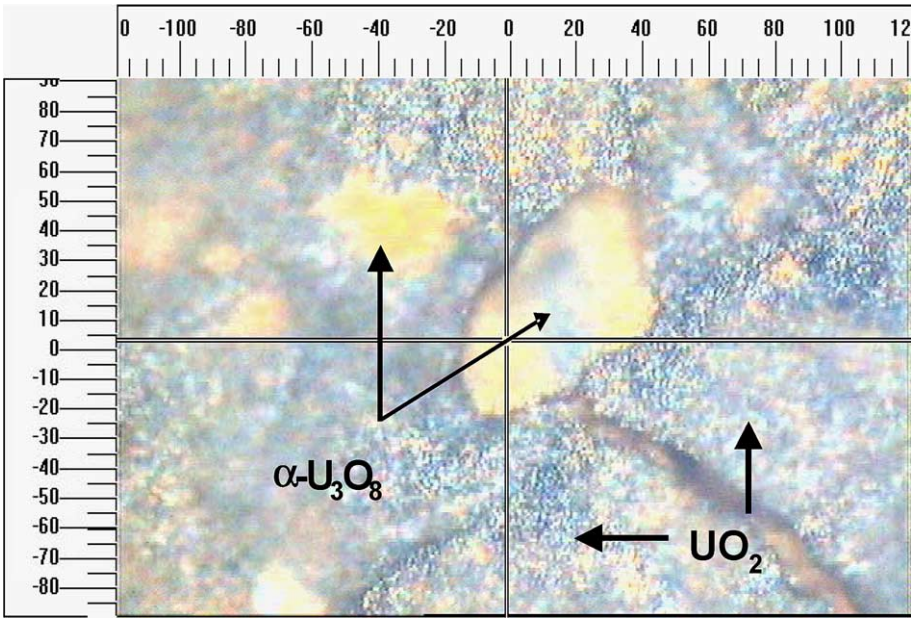

Fig. 4. Optical microscope image of polycrystalline UO_2 upon exposure to H_2O vapor at room temperature in the Raman cell. Lighter regions identified from Raman spectroscopy as α-U_3O_8, and darker regions as UO_2. The scale on both sides is in micrometer.

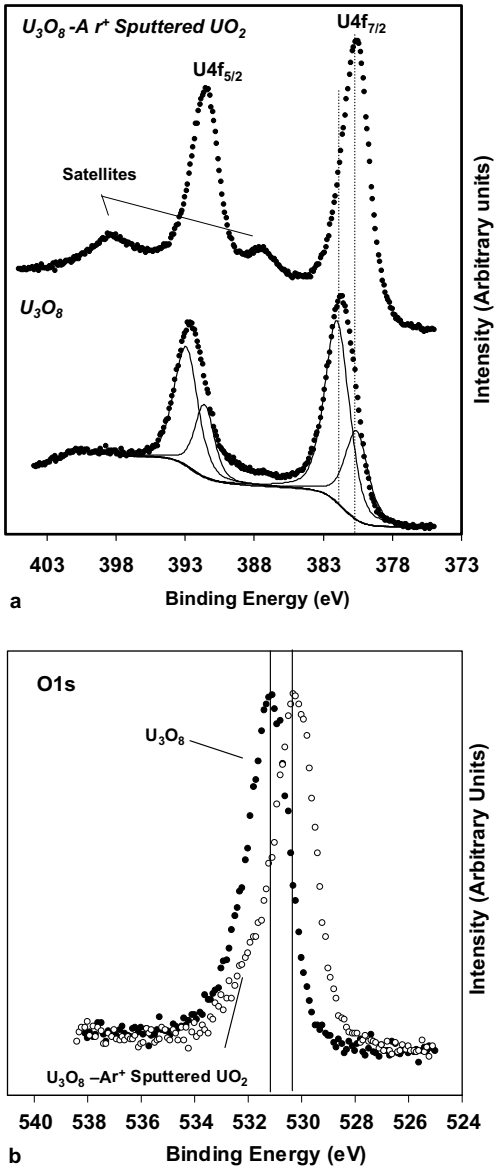

Fig. 5. (a) XPS (Al Kα) of $U4f_{7/2}$ and $U4f_{5/2}$ of α-U_3O_8 and UO_2(prepared from Ar^+ sputtering of α-U_3O_8). Peak fitting of α-U_3O_8 peak shows +4 and +6 oxidation states. (b) O1s of α-U_3O_8 and UO_2(prepared from Ar^+ sputtering of α-U_3O_8). Darker filled dots correspond to α-U_3O_8, and lighter unfilled dots of UO_2.

to U ratio in this case as equal to 2. However, we wanted to see the effect of sputtering time on the reduction of U_3O_8 to UO_2 and to UO_{2-x}. In that regard we have conducted several Ar^+-sputtering experiments (as a function of sputtering time) and have found that the ratio O to U decreased fast and then showed a very slow decrease with increasing sputtering time. Fig. 6 shows the effect of Ar^+-sputtering on the corrected O to U ratios (corrected using U_3O_8). It is important to emphasize that the curve is semi-quantitative since the first point (zero time) is attributed to pure U_3O_8. The trend is however clear, after few hours of sputtering the ratio changes very slowly. If we consider a correction factor of 16.1 and that the fresh U_3O_8 is a good representation than the sputtering surface after 4 h was the closest possible to UO_2 (actually $UO_{2.06}$).

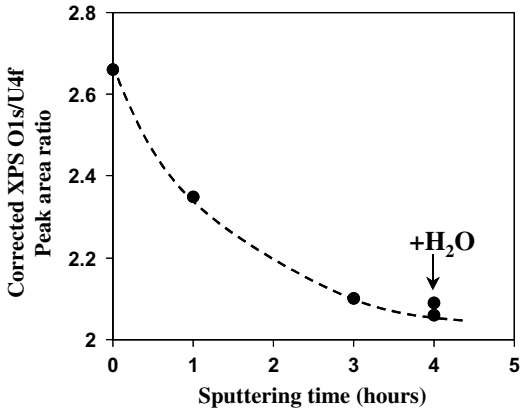

Fig. 6. Peak area ratio O1s/U4f vs Ar^+ sputtering time. Final point shows the H_2O introduced surface.

Fig. 7 shows the valence region of U_3O_8. The U_3O_8 peaks correspond to the U5f, U6d–O2p, $U6p_{3/2}$, O2s, and $U6p_{1/2}$ orbital bands at binding energy 1.0, 4.5,

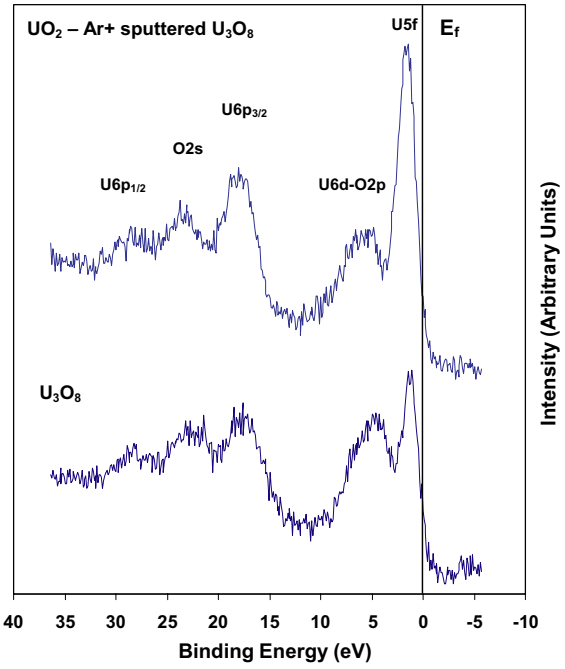

Fig. 7. XPS of valence band region of α-U_3O_8 and UO_2.

17.2, 22.4 and 28.0 eV respectively. Common to the actinide oxides the U6d and O2p bands appear as one peak due to intrinsic hybridization effect of U–O bonding. The binding energy difference of the $U6p_{3/2}$ and $U6p_{1/2}$ is found equal to 11 eV. O_2-annealed U_3O_8 shows even a smaller U5f to U6d–O2p ratio (not shown). The spectrum for the Ar^+-sputtered surfaces is also displayed. A shift to lower binding energy is noticed and associated with it an increase of the U5f to U6p–O2p peak height ratios. The shift is consistent with moving from U_3O_8 to UO_2 (both are n-type semiconductors). It is however not simple to extract information from the shift since UO_{2+x} is formed while moving from U_3O_8 to UO_2 and UO_{2+x} is a p-type semiconductor.

Water (10 L) was then dosed on the sample at 300 K and the data are analyzed by XPS. Dosing water did increase the ratio to $UO_{2.09}$ (Fig. 6). This increase is due to both water adsorption (screening) and dissociation to surface oxygen atoms. Fig. 8 shows the core level U4f before and after water adsorption. The decrease of the satellites is the most noticeable change. A slight increase of the O1s line attributed to OH species at 532.7 eV is also observed (not shown). An estimation of the amount of oxygen (and water) deposited on the surface can be obtained from the attenuation of the U4f line using the following expression [35]:

$$I_B = I_{B0} \times \left[1 - \phi_A + \phi_A \exp\left[\frac{-a_A}{\lambda(E_B)\cos\theta}\right]\right], \quad (1)$$

where I_{B0} is the U4f signal before H_2O adsorption, I_B that after H_2O adsorption, λ the attenuation length of the photoelectron (taken as 10 Å) and θ is the angle to the analyzer (50°). ϕ is found equal to ≈0.2; this number is only an estimation since the attenuation of the U4f lines attributed to U^{4+} due to water adsorption (screening) will compete with other U^{4+} ions that might have been formed as a result of water dissociation and the consequent oxidation of U^{x+} to U^{4+}.

TPD of D_2O was conducted on ≈UO_2 to see for the extent of surface oxidation. Water dissociation, associated with D_2/H_2 formation, has been recently studied by our group [3] and Paffett group [12] on oxygen defected UO_2 single crystals. We have seen two/three desorption temperatures for hydrogen (the third one is seen at very high surface exposure). Our main

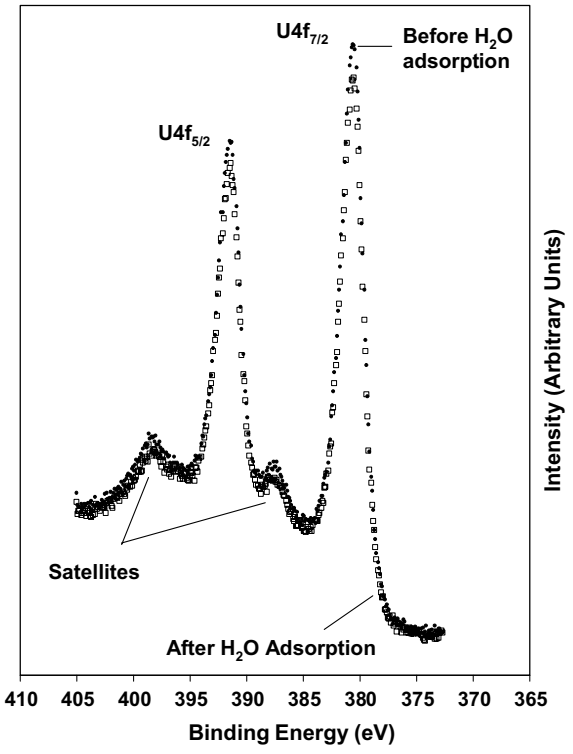

Fig. 8. XPS of $U4f_{7/2}$ and $U4f_{5/2}$ of clean UO_2 surface before and after introduction of H_2O vapor. Surface before adsorption appears as dark filled dots and after H_2O as unfilled lighter colored squares.

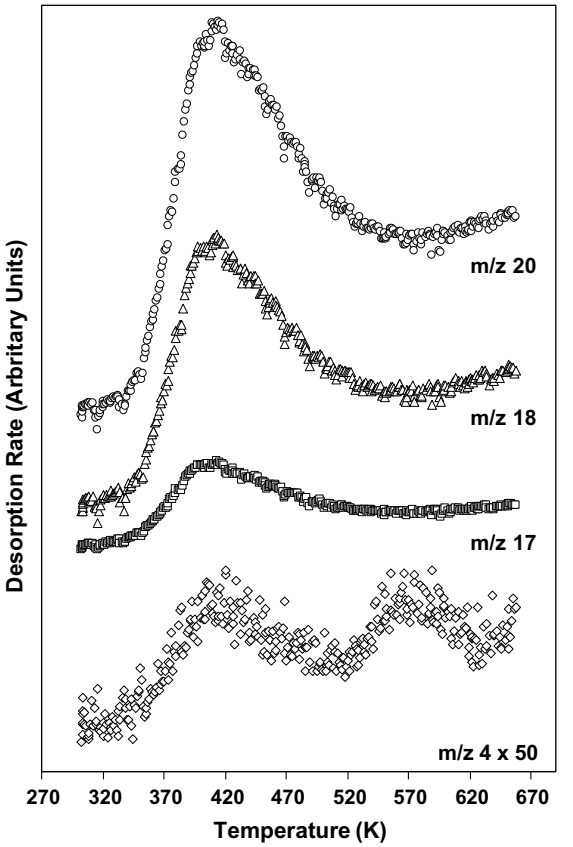

Fig. 9. TPD profile of D_2O on clean UO_2 surface. Desorption profiles stacked for clarity.

conclusion for the defected UO_2 single crystal works was that the high temperature desorption peak populated second. This could be explained as due to hydrogen–hydrogen recombination from deeper layers (where hydrogen molecules have to cross another activation barrier before desorbing). Fig. 9 shows TPD results following 1 μl adsorption of D_2O on UO_2. The BET surface area of UO_2 is close to 3.5 m^2 for the 0.5 g used during TPD. This is equivalent to 3.5×10^{19} atoms (of which two-thirds are O and one-third is U atoms). One microliter of D_2O contains 3.3×10^{19} molecules. In other words a ratio 3 to 1 of D_2O to U.

As shown in Fig. 9 there are two desorption peaks of D_2, the first one at 410 K and the second one at 570 K. While D_2O, and some H_2O, also desorbed at 420 K. Fig. 10 shows the effect of increasing the initial surface exposure (above surface saturation) on D_2 evolution during TPD. The second peak for D_2 increases considerably with increasing surface exposure to D_2O. Combining this observation with that of Raman results indicates that the second desorption peak translates a farther reaction of UO_2 with D_2O. The higher the D_2O exposure the more likely is the surface to bulk O and H atoms diffusion to occur. The reaction sequence can be described as follows.

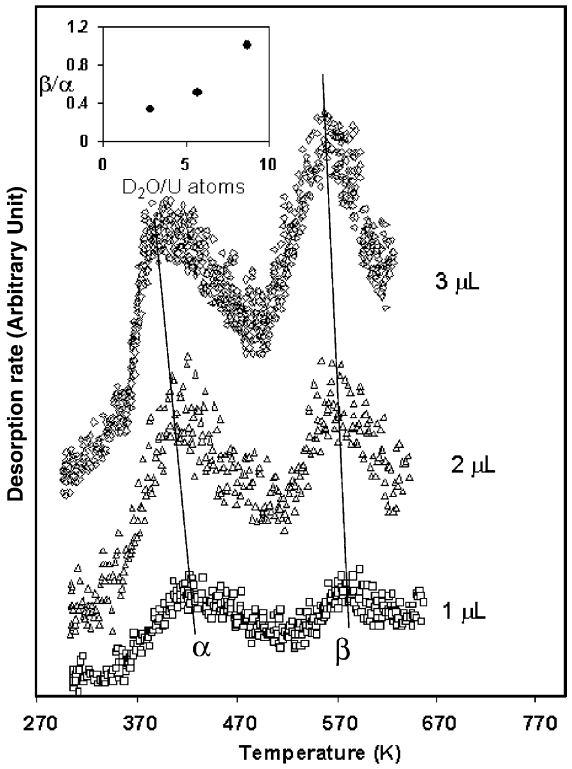

Fig. 10. TPD profiles of D_2 desorption with increasing coverage (1–3 μL). Inset shows β/α vs D_2O/ U atom.

D_2O dissociation:

$$D_2O(a) \rightarrow D(a) + OD(a), \quad (2)$$

$$D(a) + OD(a) \rightarrow D_2O(g)\ 410\ K\ \text{(recombination)}. \quad (3)$$

DO dissociation to deuterium (D) and Oxygen (O) atoms:

$$OD(a) \rightarrow D(a) + O(a). \quad (4)$$

Surface D atoms recombination:

$$2D(a) \rightarrow D_2(g)\ \text{at}\ 410\ K - \text{first layer}. \quad (5)$$

Diffusion of D atoms from deeper layers followed by recombination

$$2D(a) \rightarrow D_2(g)\ \text{at}\ 550\ K\ \text{and above} \quad (6)$$

(a) absorbed, (g) gas phase.

4. Conclusions

By combining Raman spectroscopy with XPS and TPD it was possible to track the oxidation of UO_2 using water. While Raman showed that some parts of UO_2 could be oxidized to U_3O_8 at 300 K with water vapor, XPS showed that part of the surface was oxidized with an overall stoichiometry equal to $UO_{2.09}$. D_2O-TPD showed the evolution of two D_2 desorption peaks with a distribution dependent on the initial surface exposure. The first desorption did saturate first while the second desorption increased with increasing initial surface exposure. This second desorption is due to D_2 desorption from deeper layer and is consistent with the Raman results.

Acknowledgements

The authors would like to acknowledge the contribution of Dr John Sekins for his assistance with Raman spectroscopy, Peter Buchanan and Dave Newton for technical assistance. S.D. Senanayake also wishes to thank RISIS Pte Ltd. for financial contribution, the University of Auckland for Graduate Research Fund, Partnership Appeal Award and Vice Chancellors Strategic Development Award Doctoral Scholarship.

References

[1] S.D. Senanayake, S.V. Chong, H. Idriss, Catal. Today 85 (2003) 311.
[2] S.D. Senanayake, S.V. Chong, H. Idriss, Stud. Surf. Sci. Catal. 145 (2003) 363.
[3] S.D. Senanayake, H. Idriss, Surf. Sci. 563 (2004) 135.
[4] H. Madhavaram, H. Idriss, J. Catal. 224 (2004) 358.
[5] H. Madhavaram, H. Idriss, J. Catal. 184 (1999) 553.
[6] S.V. Chong, H. Idriss, J. Vac. Sci. Tech. A 19 (2001) 1933.

[7] S.V. Chong, T.R. Griffiths, H. Idriss, Surf. Sci. 444 (2000) 187.
[8] S.V. Chong, H. Idriss, Surf. Sci. 444 (2000) 187.
[9] S.V. Chong, H. Idriss, Surf. Sci. 504 (2002) 145.
[10] H. Madhavaram, H. Idriss, J. Vac. Sci. Tech. A 153 (2) (1997) 1685.
[11] M.N. Hedhili, B.V. Yakshinskiy, T.E. Madey, Surf. Sci. 445 (2000) 512.
[12] J. Stultz, M.T. Paffett, S.A. Joyce, J. Phys. Chem. B 108 (2004) 2362.
[13] M. Balooch, A.V. Hamza, J. Nucl. Mater. 230 (1996) 259.
[14] W.L. Manner, J.A. Lloyd, M.T. Paffett, J. Nucl. Mater. 275 (1999) 37.
[15] M.T. Paffett, D. Kelly, S.A. Joyce, J. Morris, K. Veirs, J. Nucl. Mater. 322 (2003) 45.
[16] H.R. Hoekestra, S. Siegel, J. Inorg. Nucl. Chem. 18 (1961) 166.
[17] P.A. Thiel, T.E. Madey, Surf. Sci. Rep. 7 (1987) 211.
[18] M.A. Henderson, Surf. Sci. Rep. 46 (1–8) (2002) 1.
[19] K. Winer, C.A. Colmenares, R.L. Smith, F. Wooten, Surf. Sci. 183 (1987) 67.
[20] I.S. Butler, G.C. Allen, N.A. Tuan, Appl. Spec. 42 (5) (1988) 901.
[21] G.C. Allen, I.S. Butler, N.A. Tuan, J. Nucl. Mater. 144 (1987) 17.
[22] P.R. Graves, Appl. Spec. 44 (1990) 1665.
[23] M.L. Palacios, S.H. Taylor, Appl. Spec. 54 (2000) 1372.
[24] J. Schoenes, J. Chem. Soc. Faraday Trans. 283 (1987) 1205.
[25] D.P. Armstrong, R.J. Jarabek, W.H. Fletcher, Appl. Spec. 43 (1989) 461.
[26] G.M. Begun, R.G. Haire, W.R. Wilmarth, J.R. Peterson, J. Less-Comm. Metals 162 (1990) 129.
[27] M. Amme, B. Renker, B. Schmid, M.P. Feth, H. Bertagnolli, W. Döbelin, J. Nucl. Mater. 306 (2002) 202.
[28] D. Manara, B. Renker, J. Nucl. Mater. 321 (2003) 233.
[29] G. Dolling, R.A. Cowley, A.D.B. Woods, Can. J. Phys. 43 (1965) 1397.
[30] B.O. Loopstra, Acta Cryst. 17 (1964) 651.
[31] K. Ohwada, T. Soga, Spectrochim. Acta. 29 A (1973) 843.
[32] R.J. Ackermann, A.T. Chang, C.A. Sorrell, J. Inorg. Nucl. Chem. 39 (1977) 75.
[33] A.C.S. Sabioni, W.B. Ferraz, F. Milo, J. Nucl. Mater. 278 (2000) 364.
[34] J.F. Moulder, W.F. Stickle, P.E. Sobol, K.D. Bomben, in: J. Chastain (Ed.), Handbook of X-ray Photoelectron Spectroscopy, Perkin Elmer Corporation, Eden Prairie, MN, USA, 1992.
[35] G. Ertl, J. Kuppers, Low Energy Electrons and Surface Chemistry, second ed., VHC, Weinheim, 1985.